Progress In Electromagnetics Research, Vol. 141, 577–590, 2013

FREE-SPACE AND ON-METAL DUAL-BAND TAG FOR UHF-RFID APPLICATIONS IN EUROPE AND USA

Ferran Paredes[1, *], Gerard Zamora[1], Simone Zuffanelli[1], Francisco J. Herraiz-Martinez[2], Ferran Martín[1], and Jordi Bonache[1]

[1]GEMMA/CIMITEC, Departament d'Enginyeria Electrònica, Universitat Autònoma de Barcelona, BELLATERRA, Barcelona 08193, Spain

[2]Department of Signal Theory and Communications, Carlos III University in Madrid, Leganés, Madrid 28911, Spain

Abstract—In this paper, we present an UHF-RFID tag mountable on metallic surfaces and capable to operate in the assigned frequency bands in Europe (866–869 MHz) and USA (902–928 MHz). Due to the proximity of these frequency bands, the dual-band functionality can be achieved through a perturbation method applied to a single band tag designed to operate at the intermediate frequency. The tag consists of an integrated circuit, an impedance matching network (where the perturbation method is applied) and a patch antenna. The considered antenna has been chosen because it has high efficiency over metallic surfaces. The whole tag has been analyzed, designed and finally fabricated. The read ranges measured in free-space are 9.5 m and 7.5 m at the European and USA frequency bands, respectively. By placing the tag on a metal surface, the read ranges increase up to 14 m and almost 11 m, respectively.

1. INTRODUCTION

Radio frequency identification (RFID) is a technique used for identification and tracking of objects by means of electromagnetic waves [1]. Such a technology has become very popular in the recent years, and it covers different spectrum locations in the ultra high frequency (UHF) band, according to worldwide regulations. Thus, Europe operates at 866–869 MHz, USA at 902–928 MHz, and Japan at 950–956 MHz [2], to cite some of the assigned bands.

Received 13 May 2013, Accepted 22 June 2013, Scheduled 5 August 2013

* Corresponding author: Ferran Paredes (ferran.paredes@uab.es).

The RFID system consists of an interrogator, namely the reader [3], and the tags [4] that contain relevant information of the objects they are attached. The reader sends a modulated signal in all directions, and the tags located within the reader read range must be capable to receive the signal and generate a backscatter to the reader. Most used tags are based on plastic substrates, namely inlays [5, 6]. However, it is known that the performance of inlays close to liquids or mounted on metallic surfaces is severely degraded [7, 8], which results in read ranges of only few centimeters. To circumvent this limitation, specific tags, able to operate in metallic environments, have been designed. Thus, metallic tags keep their functionality when they are attached on any surface, including metals. One of the key issues of metallic tags is the tradeoff between the on-metal performance and the antenna height. Low-profile antennas, based on meandered patch antennas [9] or planar inverted-F antennas (PIFA) [10] have low performance and as a consequence the operation ranges are less than four meters. As compared to inlays or low profile antennas, metallic tags have long read ranges and major robustness, but they have larger dimensions.

Patch antennas [11, 12] are considered for RFID applications because they exhibit high radiation efficiency, regardless of the surface where the tag is attached. Moreover, patch antennas can be directly matched to the integrated circuit through conjugate matching [13], although the matching is only achieved at one frequency band. In [14] a long range metallic tag was proposed, where 14 meters of read range was achieved at European band. Similarly, in [15] a metallic tag was designed and the read range reached about 24 meters in the USA band, due to the smaller threshold power of the chip. In order to achieve long read ranges in two different UHF-RFID regulated frequency bands, it is convenient to cascade a dual-band matching network between the antenna and the chip [16]. Thus, the novelty of this work is the design of a dual-band UHF-RFID tag by means of an impedance matching network. Such tag exhibits very reasonable read ranges at the operating bands, regardless of the surface where the tag is attached, including metal surfaces.

2. DESIGN OF THE DUAL BAND TAG

2.1. Design of Microstrip Patch Antenna

Microstrip patch antennas (MPA) use printed-circuit technology and they are based on a conducting patch printed on top of a grounded layer. Thanks to the presence of such ground plane, the MPA exhibits its functionality on any surface. The advantages of MPAs are low

profile, light weight, low cost, but inherent narrow bandwidth [12]. Nevertheless, bandwidth can be broadened by increasing the thickness of the substrate.

A canonic square shape patch antenna has only two geometric parameters, the width W and the length L. A wider width increases the antenna gain, but it also increases the dimensions and the difficulty to match the input impedance. The length directly affects to the operation frequency. An arbitrary antenna geometry 60 mm × 60 mm patch antenna is designed on the *Rogers RO3010* substrate with dielectric constant $\varepsilon_r = 10.2$ and thickness $h = 1.27$ mm. An air gap with thickness 5 mm is added between the antenna substrate and ground by means of holders and posts. Such air gap decreases the effective dielectric constant, thus improving bandwidth and radiation efficiency [17]. By etching a slot in the patch (Fig. 1), the current distribution changes because the current lines must increase their trajectories, and consequently, the operation frequency shifts down [18]. Such effect can be noticed in the input impedance of the antenna and in the reflection coefficient as well, where the antenna without the slot is shifted up by 600 MHz (Fig. 2). The radiation patterns are represented in Fig. 3. Due to the presence of a ground plane, the antenna without slot has a directive pattern with 7.7 dB gain at broadside, whereas the antenna with slot has a directive pattern of 8 dBi. It is important to point out that the software used (*ADS*

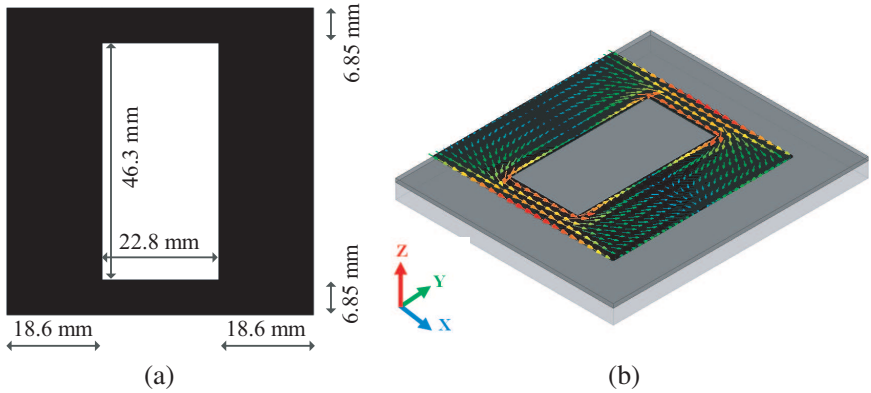

Figure 1. (a) Dimensions of the 60 mm × 60 mm patch antenna, where the slot is etched in the center of the patch and its dimensions are 46.3 mm width and 22.8 mm length. (b) Current distribution. The *Rogers RO3010* substrate and the 5 mm air gap are depicted in dark and light grey, respectively.

Agilent Momentum) considers an infinite ground plane, so the patterns correspond to the case of the antennas attached on metallic surfaces.

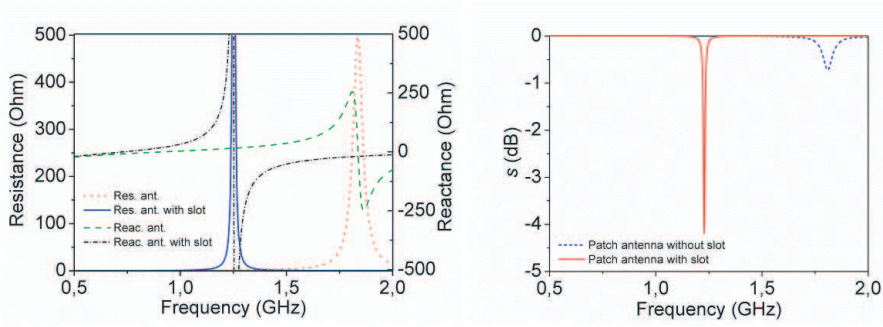

Figure 2. (a) Input Impedance and (b) reflection coefficient of the patch antenna with and without the slot.

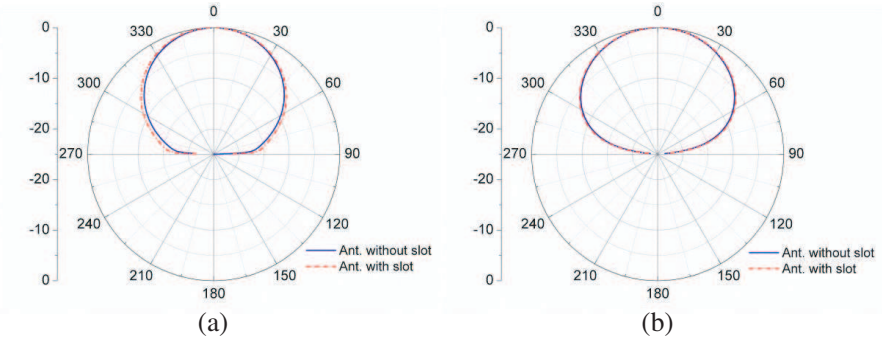

Figure 3. (a) Radiation pattern of the designed patch antennas for electric plane XZ and (b) for magnetic plane YZ. The normalized gains are 7.7 dBi and 8 dBi for the patch antenna without slot and the same antenna with slot, respectively.

In order to tailor the dual-band impedance matching network in the next section, the effective dielectric constant is required and it can be obtained by means of

$$\varepsilon_{eff} = \left(\frac{c}{v_p}\right)^2 = \left(\frac{c\beta l}{2\pi f l}\right)^2 = \left(\frac{c\theta}{2\pi f l}\right)^2 \tag{1}$$

where c is the speed of light in vacuum, v_p the phase velocity, βl the electrical length (denoted as θ), f the frequency, and l the physical length of the considered line. By simulating a microstrip line with

11.5 mm width and 46.8 mm length, and by means of (1), the final substrate can be considered to have an effective dielectric constant $\varepsilon_{eff} = 1.9$ around of the interest frequencies, and a thickness of $h = 6.27$ mm (substrate layer plus air gap). In order to reduce the tag costs, the *Rogers RO3010* substrate can be replaced with *FR4*, although it represents an 8% increase in dimensions. The best choice is to use an homogenous and cheap substrate with a low dielectric constant or high-density polyethylene (HDPE) foam [7]. The width and the length of the line used to calculate the effective dielectric constant have been chosen according to the dimensions of the impedance matching network, as will be seen in the next section.

2.2. Design of the Dual-band Impedance Matching Network

Following [16], the dual-band impedance matching network, based on a transmission line loaded with a resonator, is cascaded between the antenna and the chip. First of all, the values of the resistance and the reactance of the antenna at the frequencies of interest must be considered (Fig. 2). The antenna impedance values are $Z_a(f_1) = 0.35 + j12.7\,\Omega$ and $Z_a(f_2) = 0.45 + j18.5\,\Omega$. From the datasheet of the considered chip (the *SL3S1001* from *NXP semiconductors*), the integrated circuit impedances are $Z_{IC}(f_1) = 20.5 - j500\,\Omega$ and $Z_{IC}(f_2) = 19.5 - j471\,\Omega$. The requirements for the dual-band impedance matching network can be obtained by forcing conjugate matching, that is

$$Z^*_{IC}(f) = Z_B(f)\frac{Z_A(f) + jZ_B(f)\tan\beta l}{Z_B(f) + jZ_A(f)\tan\beta l} \tag{2}$$

where Z_{IC} is the integrated circuit impedance, Z_A the antenna input impedance, and Z_B and βl are the characteristic impedance and electrical length of the dual-band impedance matching network, respectively. The right member in (2) is the impedance seen from the chip terminals looking into the impedance matching network. From (2), we obtain a characteristic impedance $Z_{B1} = 64.4\,\Omega$ and an electrical length $\phi_1 = \beta l = 71.6^\circ$ at f_1, and $Z_{B2} = 71.3\,\Omega$ and $\phi_2 = \beta l = 66.8^\circ$ at f_2.

The parameters of the transmission line matching network can be obtained by evaluating the arithmetical mean of the characteristic impedance and electrical length at the intermediate frequency (891 MHz). By means of the effective dielectric constant and thickness, the geometry of the line (width and length) can be determined. Hence, at the intermediate frequency we obtain $Z_{B0} = 67.8\,\Omega$ and $\phi_0 = \beta l = 69.2^\circ$, which corresponds to a line width of 11.5 mm and a line length of 46.8 mm. Concerning the resonator, its topology can be

found according to the characteristic impedances at the frequencies of interest (Z_{B1} and Z_{B2}). From such values, it can be observed a positive or negative trend, which can be associated with an equivalent circuit and consequently, related with the suitable resonator topology [19]. Regarding the electrical length, it allows to find the coupling to the line, regardless of the resonator topology. In this case, due to the positive trend of the characteristic impedances ($Z_{B1} < Z_{B2}$), a shunt LC resonant tank (i.e., the complementary split ring resonator — CSRR [20]) should be applied to the transmission line to satisfy the impedance requirements. Nevertheless, the CSRR must be avoided because it involves etching the ground plane, and as a consequence, it would increase the complexity of the tag fabrication process. Hence, a split ring resonator (SRR) [21, 22] is employed (it can be etched on the top layer). The SRR can be modeled as a series connected parallel LC tank (rather than a shunt tank) from which it follows that $Z_{B1} > Z_{B2}$, i.e., contrary to our requirements. Nevertheless, this negative trend does not represent a significant degradation of the read range.

According to the perturbation method reported in [16], by means of the electrical length and the characteristic impedance, the SRR reactance at the operating frequencies is found to be $\chi_{f1} = -\chi_{f2} = 10.09\,\Omega$. It corresponds to an inductance of $L'_s = 97.2\,\text{pH}$ and a capacitance of $C'_s = 328\,\text{pF}$ from the lumped equivalent model of the SRR coupled to the microstrip line [23]. The geometric parameters of the resonator (c, d, r_{ext} and r_{in}), which are shown in Fig. 4, are determined according its equivalent model in order to obtain the resonant frequency at 891 MHz, but as usual, we optimized the final geometry. Concerning to the distance l_{SRR} between the host

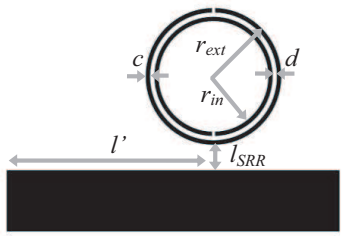

Figure 4. Layout of the impedance matching network. The width of the line is 11.5 mm and the length 46.8 mm. The resonator has an internal radius $r_{in} = 7.8\,\text{mm}$, external radius $r_{ext} = 8.7\,\text{mm}$, rings width $c = 0.5\,\text{mm}$, inter-rings distance $d = 0.6\,\text{mm}$, distance between host line and SRR $l_{SRR} = 2.4\,\text{mm}$ and position of the SRR from the left side of the transmission line $l' = 27.4\,\text{mm}$. The integrated circuit is located at the left side of the layout, and the patch antenna at the right side.

line and the SRR, it determines the level of coupling. A strong coupling between the resonator and the host line introduces large variations in the electrical length, which tend to far the resonance frequencies. Conversely, a weak coupling produces a small split-off of both frequencies. This behavior is shown in Fig. 5(a). The characteristic impedance of the matching network is also shown, where it can be seen a smooth variation regarding the desired impedance value at the American frequencies. After the resonance frequencies are determined, an adjustment in the characteristic impedance is done by means of the distance l', which is the relative position of the resonator along the host line. Such parameter does not affect the electrical length (Fig. 5(b)), which was set and it remains unaltered, and it only affects the characteristic impedance. The effect of moving the resonator across and along the host line is also shown in Fig. 6 by means of the reflection coefficient of the impedance matching network cascaded to the patch antenna.

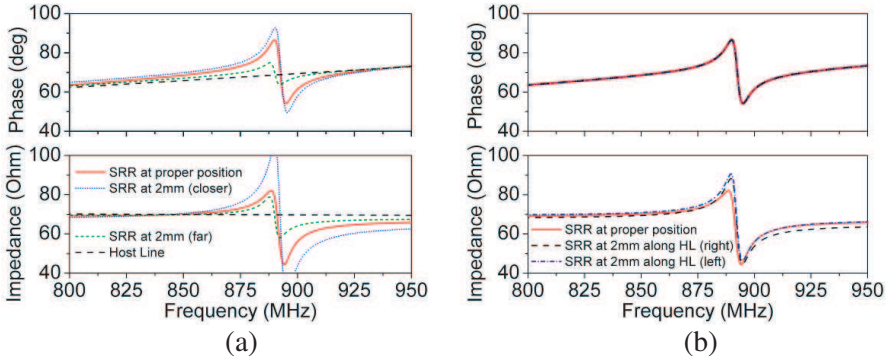

Figure 5. (a) Electrical length and characteristic impedance for the impedance matching network, where the resonator was coupled to different positions across the host line (orthogonal movement). The impedance matching network without the SRR is also shown. (b) Electrical length and characteristic impedance for the impedance matching network, where the resonator was moved along the host line.

The electrical length and the characteristic impedance of the final layout are depicted in Fig. 7. At the European frequency (867 MHz) we obtain $Z_{B1} = 71.5\,\Omega$ and $\phi_1 = \beta l = 71.1°$, and at the USA frequency (915 MHz) we obtain $Z_{B1} = 63.5\,\Omega$ and $\phi_1 = \beta l = 68.6°$. Comparing these values with the required ones, the electrical lengths are similar, which allows to adjust the resonant frequencies. As expected, for the characteristic impedance the obtained values do not

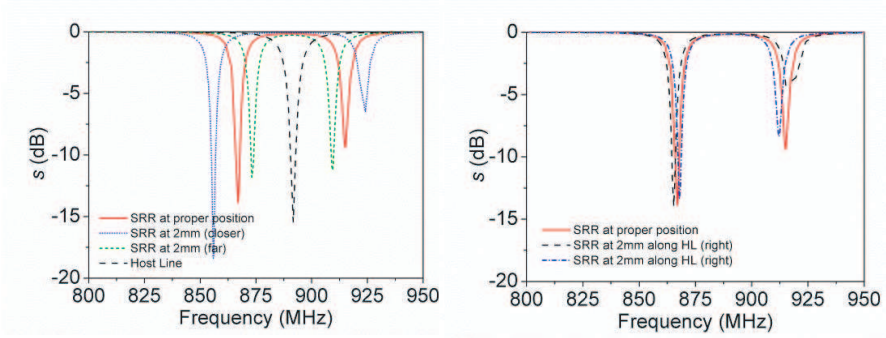

Figure 6. Reflection coefficient for the impedance matching network, where the resonator was moved orthogonal (a) or along (b) the host line.

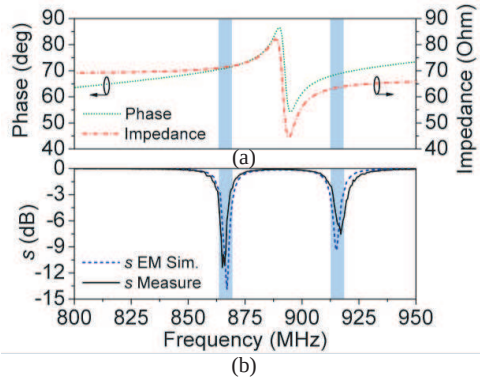

Figure 7. (a) Phase and characteristic impedance of the dual-band impedance matching network. (b) Simulated and measured power wave reflection coefficient of the dual-band tag.

coincide, but are similar to the required ones, so as to guarantee a good matching at the frequencies of interest, and hence a dual-band behavior. The power wave reflection coefficient has been obtained and also depicted in Fig. 7. A smith chart (Fig. 8) has been added to better understand the matching technique. Considering the patch antenna cascaded with the impedance matching network without the SRR, it is a host line only, impedance matching is obtained at intermediate frequency $f_0 = 891\,\text{MHz}$. According to Smith chart, it involves that the input impedance of the tag passes through the desired conjugate value. Now, we consider the impedance matching network with the

SRR located at the proper position. The SRR introduces a resonance at the intermediate frequency, which allows the input impedance to pass through the conjugate impedance at each desired frequency. The radiation patterns of the designed dual-band tag (Fig. 9), including the impedance matching network, are the same than those of the patch antenna, but due to the dual-band behavior, the efficiency and the gain have decreased. The gains are 6.3 dBi and 6.9 dBi at the European and USA frequency bands, respectively.

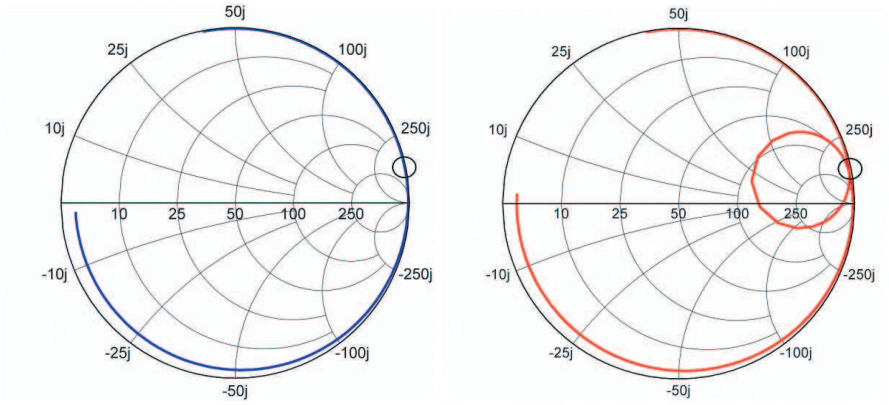

Figure 8. (a) Smith chart for the antenna cascaded with a convention line to obtain the conjugate impedance at intermediate frequency 891 MHz, and (b) smith chart for the antenna with the impedance matching network designed to provide dual-band behavior.

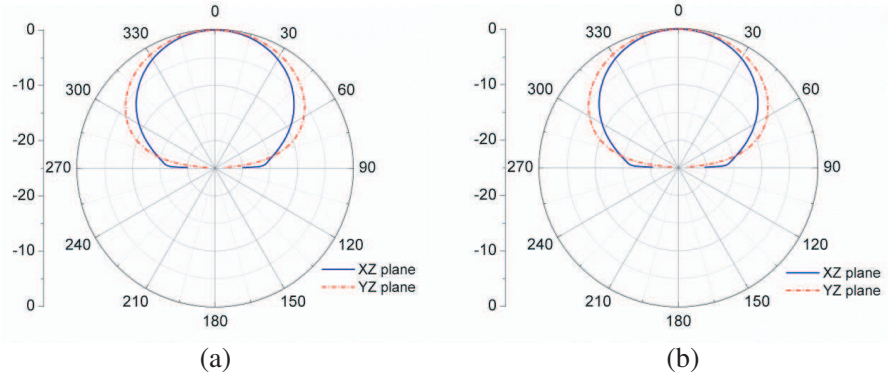

Figure 9. (a) Radiation pattern of the designed patch antennas for European frequencies, and (b) for the American frequencies. The normalized gains are 6.3 dBi and 6.9 dBi, respectively.

3. FABRICATION, MEASUREMENT AND READ RANGE

3.1. Fabrication and Measurement

The fabricated dual-band tag is shown in Fig. 10. First of all, a SMA connector was soldered between the top layer and the ground plane to measure the return loss S_{11} by means of the E8364B vector network analyzer. Since the probe impedance was $50\,\Omega$, a renormalization of the port impedance was necessary. Then, these results were exported to *Agilent ADS* in order to infer the power wave reflection coefficient s by considering the chip impedance as reference of the input port impedance (Fig. 7(b)). Good agreement was found between the simulation and the measurement. After the measurement, the SMA connector was replaced with the chip to obtain the read range.

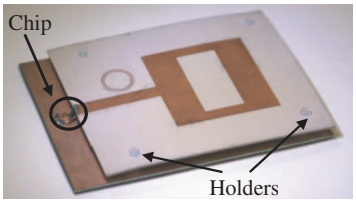

Figure 10. Photograph of the fabricated dual-band tag. Tag dimensions are $106.8\,\text{mm} \times 60\,\text{mm}$. The ground plane layer is separated from the top layer by means of posts and holders.

3.2. Read Range

The read range [24] is the fundamental parameter relative to tag performance. It can be calculated using the Friis free space formula as

$$r = \frac{\lambda}{4\pi}\sqrt{\frac{EIRPG_r\tau}{P_{chip}}} \tag{3}$$

where λ is the wavelength, *EIRP* (equivalent isotropic radiated power) determined by local country regulations, P_{chip} the minimum threshold power necessary to activate the RFID chip, G_r the gain of the receiving tag antenna, and τ the power transmission coefficient. The value of *EIRP* in European frequencies is 3.3 W, whereas in American frequencies is 4 W. The simulated read range can be inferred from Equation (3), and it is depicted in Fig. 11. As mentioned before, it is important to emphasize that, in the electromagnetic simulation, the ground plane was considered to be infinite, which corresponds to the situation where the tag is placed on a metallic surface.

The read range can be measured by means of a reader, or by means of a specific tag test setup [25]. The RFID tag test set up available in our laboratory consists of an *Agilent N5182A* vector signal generator (where RFID frames are created), an *Agilent N9020A* signal analyzer to recover the RFID frames backscattered by the tag under test, and a TEM cell. After the tag is located inside the TEM cell, a power and frequency sweep is carried out for the RFID frames. When the frequency of the RFID frame fits within the tag operation frequency, a backscatter signal is sent. Hence, observing the backscattering, we can determine the tag power activation and operation frequencies. Finally, the received power by the chip at each frequency is related to the incident electric field intensity E_0, according to

$$P_{chip} = SA_{ef}\tau = \frac{|E_0|^2}{2\eta}\frac{\lambda^2 G_r}{4\pi}\tau \tag{4}$$

where S is the incident power density, A_{ef} the effective area of the tag antenna, and η the wave impedance (which is equivalent to $120\pi\,\Omega$). The measured read range can be inferred by introducing (4) in (3), resulting

$$r = \frac{\sqrt{60EIRP}}{E_0} \tag{5}$$

The measured free-space read range (Fig. 11) was obtained by placing the tag inside the TEM cell. The read range was found to be 9.5 m at the European frequency band and 7.5 m at the USA frequency band. Due to variation of the feeding point of the chip in the fabricated tag, a slight shift up and unbalance of read range can be seen. Increasing the length of the impedance matching network would shift down and balance the read ranges. When the tag is located on a metallic surface

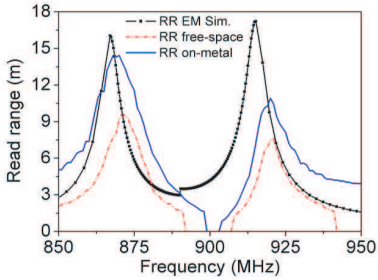

Figure 11. Read range of the dual-band tag calculated by means of the electromagnetic simulation, taking into account an infinite ground plane, and measured read range using the TEM cell (free-space), and using the TEM cell with the tag attached to a metallic slab into the cell.

of 250 mm × 250 mm, such unbalance increases. Nevertheless, the achieved read range is 14 m and almost 11 m at the European and USA bands, respectively. The agreement between the on-metal experimental and simulated read ranges is reasonable.

4. CONCLUSION

To summarize, the design of a patch-antenna based dual-band UHF-RFID tag has been carried out by means of the perturbation method applied to the impedance matching network cascaded between the chip and the patch antenna. The proposed tag has been fabricated, and the read range has been measured in free-space and with the tag attached to a metallic surface. The read ranges in free-space are 9.5 m at the European frequency band and 7.5 m at the USA frequency band. Reasonable agreement has been found between simulation and experimental results for the read range of the tag placed on top of a metallic surface, reaching 14 m at the European band, and almost 11 m at the USA band.

ACKNOWLEDGMENT

This work has been supported by Spain-MICIIN (project contracts TEC2010-17512 METATRANSFER and CSD2008-00066) and Spain MITyC through the projects TSI-020100-2009-778 and TSI-020100-2010-493. Thanks are also given to the Catalan Government for giving support through the project 2009SGR-421.

REFERENCES

1. Kim, M. and K. Kim, "Automated RFID-based identification system for steel coils," *Progress In Electromagnetics Research,* Vol. 131, 1–17, 2012.
2. Hunt, V. D., A. Puglia, and M. Puglia, *RFID: A Guide to Radio Frequency Identification,* John Wiley & Sons, Inc., New York, 2007.
3. Lai, X.-Z., Z.-M. Xie, and X.-L. Cen, "Design of dual circularly polarized antenna with high isolation for RFID application," *Progress In Electromagnetics Research,* Vol. 139, 25–39, 2013.
4. Chen, S.-L., S.-K. Kuo, and C.-T. Lin, "A metallic RFID tag design for steel-bar and wire-rod management application in the steel industry," *Progress In Electromagnetics Research*, Vol. 91, 195–212, 2009.

5. Catarinucci, L., R. Colella, and L. Tarricone, "Smart prototyping techniques for UHF RFID tags: electromagnetic characterization and comparison with traditional approaches," *Progress In Electromagnetics Research,* Vol. 132, 91–111, 2012.
6. Amin, Y., Q. Chen, L.-R. Zheng, and H. Tenhunen, "Development and analysis of flexible UHF RFID antennas for 'green' electronics," *Progress In Electromagnetics Research,* Vol. 130, 1–15, 2012.
7. Deavours, D. D., "Improving the near-metal performance of UHF-RFID tags," *Proc. IEEE Inter. Conf. on RFID*, 187–194, Orlando, USA, Apr. 2010.
8. Amin, Y., Q. Chen, H. Tenhunen, and L.-R. Zheng, "Performance-optimized quadrate bowtie RFID antennas for cost-effective and eco-friendly industrial applications," *Progress In Electromagnetics Research,* Vol. 126, 49–64, 2012.
9. Chen, H. D. and Y. H. Tsao, "Low-profile meandered patch antennas for RFID tags mountable on metallic objects," *IEEE Antennas and Wireless Propagation Letters*, Vol. 9, 118–121, 2010.
10. Chen, H. D. and Y. H. Tsao, "Low-profile PIFA array antennas for UHF band RFID tags mountable on metallic objects," *IEEE Trans. Antennas and Propagation*, Vol. 58, No. 4, 1087–1092, 2010.
11. Tiang, J.–J., M. T. Islam, N. Misran, and J. S. Mandeep, "Circular microstrip slot antenna for dual-frequency RFID application," *Progress In Electromagnetics Research,* Vol. 120, 499–512, 2011.
12. James, J. R., *Handbook of Microstrip Antennas*, IEE Electromagnetic Wave Series 28, London, 1989.
13. Loo, C.-H., K. Elmahgoub, F. Yang, A. Z. Elseherbeni, D. Kajfez, A. A. Kishk, T. Elseherbeni, L. Ukkonen, L. Sydanheimo, M. Kivikoski, S. Merilampi, and P. Ruuskanen, "Chip impedance matching for UHF RFID tag antenna design," *Progress In Electromagnetics Research,* Vol. 81, 359–370, 2008.
14. Popov, A., S. Dudnikov, and A. Mikhaylov, "Passive UHF RFID tag with increased read range," *Proc. European. Microw. Conf.*, 1106–1108, Amsterdam, Netherlands, Oct. 2008.
15. Björnien, T., K. Espejo, L. Ukkonen, A. Z. Elsherbeni, and L. Sydänheimo, "Long range metal mountable tag antenna for passive UHF RFID systems," *Proc. IEEE Inter. Conf. on RFID Tech. and Appl.*, 202–206, Sitges, Spain, Sept. 2011.
16. Paredes, F., G. Z. Gonzalez, J. Bonache, and F. Martin, "Dual-

band impedance-matching networks based on split-ring resonators for applications in RF identification (RFID)," *IEEE Trans. Microw. Theory Tech.*, Vol. 58, No. 5, 1159–1166, 2010.

17. Godara, L. C., *Handbook of Antennas in Wireless Communications*, CRC Press, Florida, 2001.
18. Maci, S., G. Biffi, P. Piazzesi, and C. Salvador, "Dual-band slot-loaded patch antenna," *Proc. IEE Microw. Ant. and Prop.*, Vol. 142, No. 3, 225–232, 1995.
19. Paredes, F., G. Z. Gonzalez, J. Bonache, and F. Martin, "Perturbation method based on resonant type metamaterial transmission lines for dual-band matching networks," *Proc. Mediterranean Microw. Symp.*, 1–4, Tangier, Morocco, Nov. 2009.
20. Falcone, F., T. Lopetegi, M. A. G. Laso, J. D. Baena, J. Bonache, M. Beruete, R. Marques, F. Martin, and M. Sorolla, "Babinet principle applied to the design of metasurfaces and metamaterials," *Phys. Rev. Lett.*, Vol. 93, No. 19, 197401–197401-4, 2004.
21. Martín, F., F. Falcone, J. Bonache, R. Marqués, and M. Sorolla, "Split ring resonator based left handed coplanar waveguide," *Appl. Phys. Lett.*, Vol. 83, 4652–4654, 2003.
22. Montero-de-Paz, J., E. Ugarte-Munoz, F. J. Herraiz-Martinez, V. Gonzalez-Posadas, L. E. Garcia-Munoz, and D. Segovia-Vargas, "Multifrequency self-diplexed single patch antennas loaded with Split ring resonators," *Progress In Electromagnetics Research,* Vol. 113, 47–66, 2011.
23. Baena, J. D., J. Bonache, F. Martin, R. Marques, F. Falcone, T. Lopetegi, M. A.G. Laso, J. Garcia-Garcia, I. Gil, M. Flores, and M. Sorolla, "Equivalent circuit models for split ring resonators and complementary split rings resonators coupled to planar transmission lines," *IEEE Trans. Microwave Theory Tech.*, Vol. 53, No. 4, 1451–1461, 2005.
24. Rao, K. V. S., P. V. Nikitin, and S. F. Lam, "Antenna design for UHF RFID tags: A review and a practical application," *IEEE Trans. Antennas Propagation*, Vol. 53, No. 12, 3870–3876, 2005.
25. Nikitin, P. V. and K. V. S. Rao, "Theory and measurement of backscattering from RFID tags," *IEEE Antennas Propag. Mag.*, Vol. 49, No. 2, 212–218, 2006.